CONVOLUTIONAL NEURAL NETWORK FOR HOMOGENIZATION OF PARTICULATE COMPOSITE MATERIALS BASED ON FINITE ELEMENT DATA

Tien-Thinh Le[1,2,*]**, Quoc Dat Ha**[3]**, Huan Thanh Duong**[4]

Faculty of Mechanical Engineering and Mechatronics, Phenikaa University,
Yen Nghia, Ha Dong, Hanoi, Vietnam
[2]*Phenikaa Research and Technology Institute (PRATI), A&A Green Phoenix Group JSC,*
No. 167 Hoang Ngan street, Cau Giay district, Hanoi, Vietnam
[3]*Vietnam Petroleum Institute (VPI), 167 Trung Kinh street, Cau Giay district, Hanoi, Vietnam*
[4]*Faculty of Engineering, Vietnam National University of Agriculture,*
Trau Quy, Gia Lam, Hanoi, Vietnam
*E-mail: thinh.letien@phenikaa-uni.edu.vn

Abstract. This study develops a convolutional neural network model to predict the apparent mechanical properties of particulate composite materials based on finite element data. The particulate composite material is considered with random inclusions in size and position. The datasets for training and testing processes are generated by using a validated finite element simulation. Various parametric studies are then investigated, including model efficiency and uncertainty propagation. Moreover, the influence of the constituents and microstructure is numerically revealed based on the proposed convolutional neural network model. It is shown that the developed convolutional neural network model is capable of capturing the microstructural features and provides accurate predictions of apparent mechanical properties of particulate composite materials.

Keywords: convolutional neural network, finite element simulation, multiscale homogenization, particulate composites.

1. INTRODUCTION

The effective design and analysis of particulate composite materials play a critical role in advancing technologies in aerospace, automotive, and biomedical industries

[1]. The macroscopic mechanical properties of these materials are intrinsically linked to their microstructural features, including particle distribution, size, and interaction effects within the matrix [2]. Various homogenization techniques have been proposed to determine the overall properties of composite materials, categorized into three groups [3]: Analytical approaches, such as the Voigt and Reuss models; Semi-analytical approaches, including the Mori–Tanaka method and the Self-consistent model; and Numerical approaches, which encompass FE analysis, boundary element methods, and fast Fourier transform techniques. For instance, Barral et al. [4] combined the Mori–Tanaka scheme with the Transformation Field Analysis to study elastoplastic-viscoelastic composites. Kanaun [5] investigated elasto-plastic media with arrays of isolated inclusions by using a self-consistent scheme. In another study, Peng and Cao [6] developed 3D finite element analysis for investigating textile composites. Taut and Monchiet [7] employed fast Fourier transform technique for computing the effective properties of heterogeneous materials with spring-type interfaces. However, these approaches also exhibit several inconveniences [8]. Analytical approaches are most effective for simple, well-structured composites but fail to account for complex geometries and random inclusions. Moreover, analytical models do not explicitly capture the effects of inclusion morphology, spatial distribution, or interactions, leading to inaccurate predictions for heterogeneous materials. Besides, homogenization numerical tools, such as finite element (FE) analysis, have long been widely used for predicting these properties by simulating the response of the microstructure under various loading conditions. While FE-based methods provide accurate and reliable results, they are computationally intensive, especially for materials with complex microstructures or when subjected to parametric or multiscale studies [9].

Despite advancements in computational techniques, a significant gap exists in bridging high-fidelity simulations and computational efficiency. Traditional homogenization relies on extensive FE simulations requiring specialized expertise and significant computational resources [10]. Recent advances in deep learning [11], specifically Convolutional Neural Networks (CNNs), offer promising solutions to this problem. CNNs have demonstrated exceptional capabilities in feature extraction from image-based data, making them particularly suitable for analyzing microstructures of composite materials [12]. For instance, Li et al. [13] developed a transfer learning method to reconstruct microstructures and predict the overall properties of composite materials. Henkes et al. [14] stochastically quantified uncertainty in homogenized effective properties using polynomial chaos expansion combined with artificial neural networks. In another study, Jiang et al. [8] developed a deep neural network to investigate thermo-conductivity in unidirectional composites. Wang et al. [15] proposed three machine learning models to predict effective properties of unidirectional composites from FE dataset. Last but not least, a systematic review of deep neural network applications for composite design can be found in Wang et al. [16].

While existing studies have applied CNNs to microstructural analysis, the majority focus on classification tasks or approximate property prediction without integrating high-fidelity FE datasets. The potential of CNNs to replace FE-based homogenization in a systematic and accurate manner remains largely unexplored. This study addresses this critical gap by proposing a CNN-based homogenization framework that employs FE simulation data to predict macroscopic mechanical properties, such as Young's modulus and Poisson's ratio, directly from microstructural images of composites with random inclusions.

2. MATERIALS AND METHODS

2.1. Methodology

The methodology for this study is structured to integrate finite element data with convolutional neural network (CNN) modeling to predict apparent mechanical properties of particulate composite materials with random inclusions. The process begins with data generation using validated finite element simulationsto create a comprehensive dataset comprising microstructure images and their corresponding mechanical properties, including Young's modulus and Poisson's ratio. The next step involves data preprocessing, where the images are resized, normalized, and paired with their respective labels to ensure consistency and suitability for the CNN input. Subsequently, a CNN model is developed, designed to extract and learn microstructural features from the images while mapping them to the apparent mechanical properties. The model is then subjected to validation and testing against unseen data to evaluate its predictive accuracy and efficiency. Finally, the results are analyzed in the performance evaluation stage, focusing on model efficiency and the numerical influence of the microstructural characteristics. The methodology flowchart of the study is shown in Fig. 1.

2.2. Description of microstructure and finite element model

We examine a composite microstructure consisting of two phases: a matrix and a set of particle reinforcements. The matrix has a length L, while the inclusions have a diameter d_i. These inclusions are randomly distributed within the matrix, with their reinforcement fraction represented by f. From a mechanical perspective, all phases within the domain are assumed to follow linear elasticity. The Young's modulus and Poisson's ratio for the matrix are denoted as E_m and v_m, respectively, while for the inclusions, they are denoted as E_i and v_i.

The random distribution of inclusions within the domain is subject to conditions to maintain structural consistency:

- The inclusions are randomized in both size and position;

- The inclusions do not intersect the edges of the matrix (contact is permitted);

- The inclusions neither intersect nor come into contact with one another, avoiding stress concentration effects.

In the finite element model, quadrilateral elements have been employed to discretize the domain. The displacement field passing through the interface between the matrix and the inclusion was assumed to be continuous. A mesh convergence study has been done to determine the appropriate size of the mesh for the considered problem.
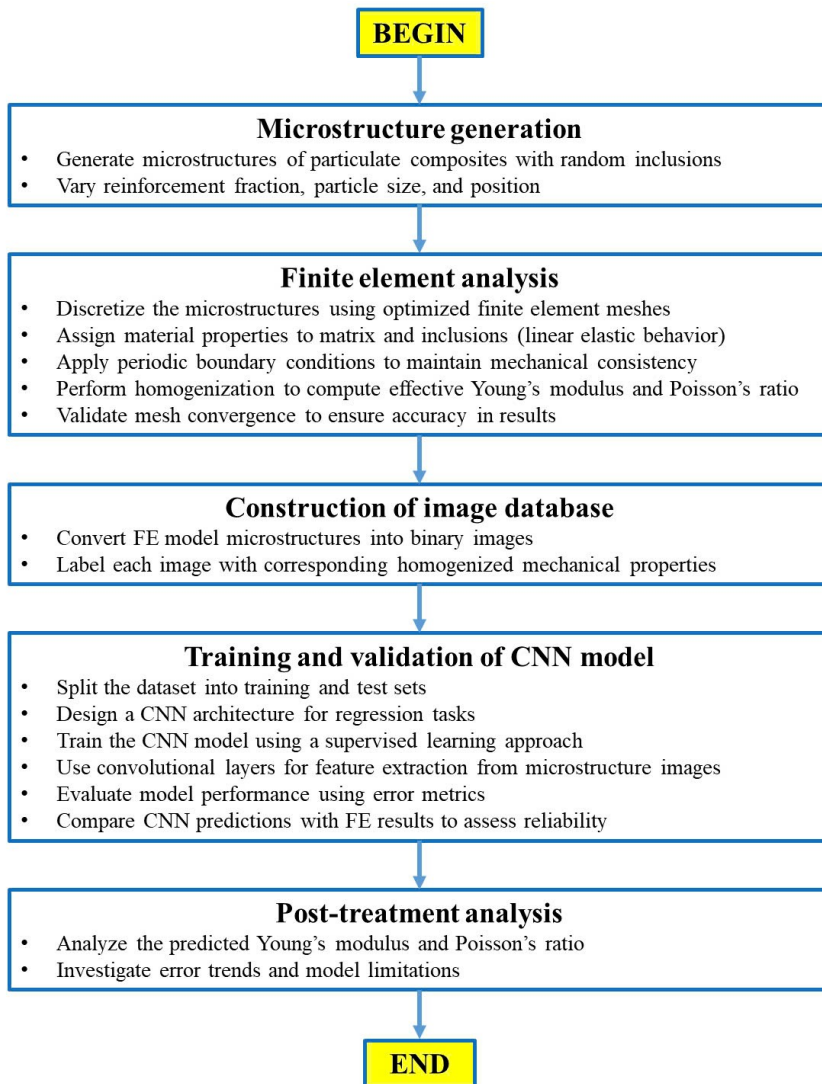
Fig. 1. Methodology flowchart of the study

2.3. Homogenization scheme and boundary condition

The homogenization scheme aims to compute the apparent mechanical properties of particulate composite materials by averaging the microstructural response over a representative volume element (RVE) [17]. To homogenize the mechanical behavior, the displacement field $\mathbf{u}(\mathbf{x})$ within the RVE is solved under specific boundary conditions, and the stress and strain fields are averaged. The effective stress tensor $\bar{\sigma}$ and strain tensor $\bar{\varepsilon}$ are calculated as

$$\bar{\sigma} = \frac{1}{V} \int_V \sigma(\mathbf{x}) \, dV, \quad \bar{\varepsilon} = \frac{1}{V} \int_V \varepsilon(\mathbf{x}) \, dV, \tag{1}$$

where V is the volume of the RVE, $\sigma(\mathbf{x})$ is the local stress tensor, and $\varepsilon(\mathbf{x})$ is the local strain tensor. Using these averaged quantities, the effective stiffness tensor $\mathbb{C}_{\text{eff}}$ can be expressed as

$$\bar{\sigma} = \mathbb{C}_{\text{eff}} : \bar{\varepsilon}. \tag{2}$$

To ensure consistency and accuracy in the homogenization process, periodic boundary conditions (PBCs) are applied to the RVE. Mathematically, for a point $\mathbf{x}$ on one boundary face of the RVE and its corresponding point $\mathbf{x}'$ on the opposite face, the displacement compatibility condition is given by

$$\mathbf{u}\left(\mathbf{x}'\right) - \mathbf{u}\left(\mathbf{x}\right) = \bar{\varepsilon} \cdot \left(\mathbf{x}' - \mathbf{x}\right), \tag{3}$$

where $\bar{\varepsilon}$ is the applied macroscopic strain tensor. This ensures that any deformation applied to the RVE maintains the periodicity of the displacement field. The corresponding traction equilibrium condition is expressed as

$$\sigma\left(\mathbf{x}\right) \cdot \mathbf{n} + \sigma\left(\mathbf{x}'\right) \cdot \mathbf{n}' = 0, \tag{4}$$

where $\mathbf{n}$ and $\mathbf{n}'$ are the outward unit normals on the respective boundaries.

In a 2D problem, the applied macroscopic strains are as below

$$\bar{\varepsilon}_{11} = \begin{bmatrix} 1 & 0 \\ 0 & 0 \end{bmatrix}, \quad \bar{\varepsilon}_{12} = \begin{bmatrix} 1/2 & 0 \\ 0 & 1/2 \end{bmatrix}, \quad \bar{\varepsilon}_{22} = \begin{bmatrix} 0 & 0 \\ 0 & 1 \end{bmatrix}. \tag{5}$$

2.4. Convolutional neural network model for regression task from images

A convolutional neural network (CNN) is a type of deep learning model designed to extract and learn features from high-dimensional data, such as images [18]. For the regression task in this study, the CNN is employed to predict the apparent mechanical properties of particulate composite materials (e.g., Young's modulus and Poisson's ratio) from microstructure images. The network processes images of composite microstructures containing randomly distributed inclusions and maps these to continuous-valued outputs representing the mechanical properties.

The input to the CNN model is an image of the microstructure, represented as a tensor of dimensions $W \times H \times C$, where W and H are the width and height of the image, and C is the number of channels (e.g., 3 for RGB images and 1 for grayscale images). The convolutional layers extract spatial features by applying filters (kernels) of size $k \times k$ to the input image. The output of a convolution operation is given by [18]

$$f_{ij} = \sum_{m=1}^{k} \sum_{n=1}^{k} w_{mn} \cdot x_{(i+m-1)(j+n-1)} + b, \tag{6}$$

where x is the input image, w is the filter, b is the bias term, and f_{ij} is the feature map at position (i, j). The filters are trained to detect features such as edges, textures, and patterns relevant to the microstructure. To train the CNN for regression, the loss function measures the error between the predicted values ($\hat{y}$) and the actual values (y) [19]

$$L = \frac{1}{N} \sum_{i=1}^{N} \left(\hat{E}_i - E_i \right)^2 + \left(\hat{v}_i - v_i \right)^2, \tag{7}$$

where N is the number of samples, E_i and v_i are the actual Young's modulus and Poisson's ratio values, and $\hat{E}_i$ and $\hat{v}_i$ are the predicted values. The CNN is trained by minimizing the loss function using gradient-based optimization methods, such as Adam or stochastic gradient descent (SGD). During training, the weights of the convolutional, pooling, and dense layers are updated iteratively to reduce the loss and improve the predictive accuracy.

3. RESULTS AND DISCUSSION

3.1. Validation of finite element model

Examples of 2 random microstructures are shown in Fig. 2 for reinforcement fractions $f = 0.30$ and $f = 0.48$. It is seen in Fig. 2 that the inclusions were generated inside the microstructure satisfying conditions introduced in Section 2.2. By using moduli of constituent materials indicated in Table 1, the finite element model for homogenization of the composite microstructure was performed on a CPU AMD Ryzen Threadripper 3970X (3.7 GHz turbo up to 4.5 GHz), 96 Gb RAM. The strain and stress fields are also shown in Fig. 2 for the 2 random microstructures, under a horizontal uniaxial tensile test. Fig. 3 presents a mesh convergence analysis for the problem, by increasing the number of finite element nodes, for both values of effective Young's modulus and Poisson's ratio of the composite. It is seen that an optimal value of mesh indicator is obtained around 200.

Fig. 4 next compares the values of effective Young's modulus and Poisson's ratio between the finite element model and experiments [1,2], for different cases of reinforcement fraction. It is interesting to notice that the Mori–Tanaka estimation is also indicated for the case of effective Young's modulus. It is seen that the numerical data are in good

agreement with the experiments. The finite element model is then used to generate microstructure images for training the convolutional neural network model.
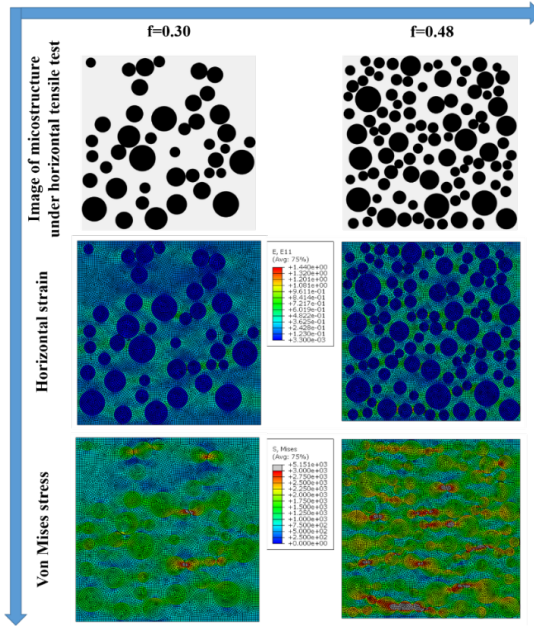
Fig. 2. Examples of 2 random microstructures with strain and stress fields, under a horizontal tensile test

Table 1. Moduli of constituent materials

Modulus	Matrix: Polymer epoxy	Reinforcement: Glass particles
Young's modulus E (GPa)	3	76
Poisson's ratio ν	0.4	0.23
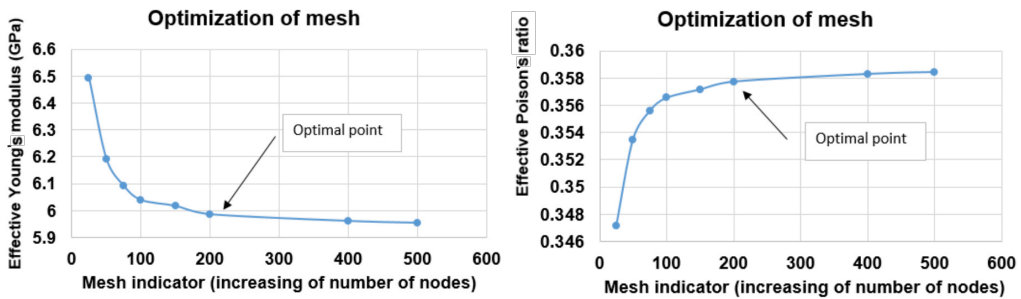
Fig. 3. Optimization of the number of nodes in the finite element domain for both effective Young's modulus and Poisson's ratio of the composite
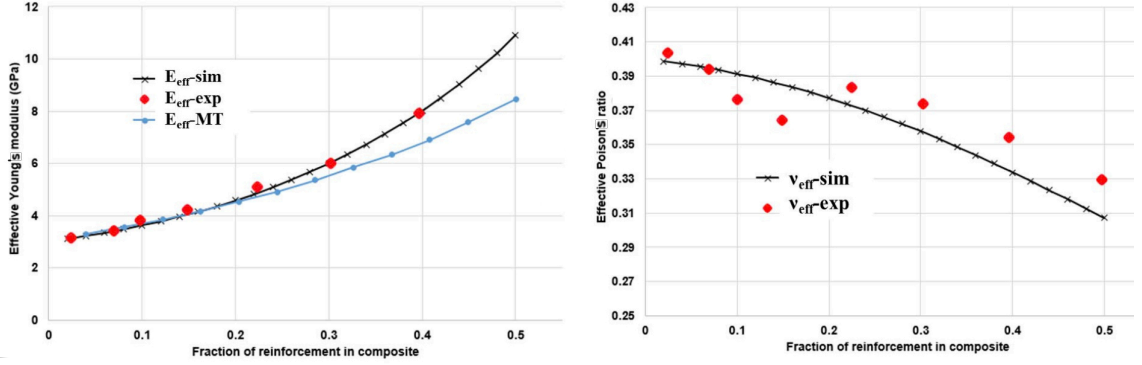
Fig. 4. Comparison of effective Young's modulus and Poisson's ratio, between the finite element model and experiments [1,2] (the Mori–Tanaka estimation is also indicated for the case of effective Young's modulus) (sim denotes the modulus from finite element simulation, exp denotes the modulus from experimentation and MT denotes the modulus from the Mori–Tanaka method)

3.2. Generation of database for images of microstructure

The microstructure images are generated from the validated finite element model with randomly distributed particle inclusions. 3000 random microstructures have been generated. The inclusions vary in size and spatial distribution to reflect realistic composite microstructures, as detailed in Section 2.2. For each configuration, the reinforcement fraction f is used as a control variable, to ensure a wide range of inclusion densities in the database. This variability enables the CNN model to learn the complex relationships between the microstructure geometry and the apparent mechanical properties. The uniform distribution was used for the value of reinforcement fraction between its minimum and maximum values, as shown in Table 2. The separation of the training and testing datasets is 70/30, i.e., 2100 images for the training stage and 900 images for the testing stage.

Table 2. Conditions for generation of database for images of microstructure

Control variable	Minimum value	Maximum value	Distribution type
Reinforcement fraction f	0.16	0.56	Uniform

Fig. 5 illustrates different random microstructures, in changing the reinforcement fraction f. Fig. 6 introduces a histogram of the diameter of reinforcements. Fig. 7 presents histogram of Young's modulus and Poisson's ratio of the composite obtained from the finite element model (the figures also indicate the modulus of the pure matrix). The associated statistical analysis of variables is indicated in Table 3, for number of data points, minimum, Q25, median, average, Q75, maximum, standard deviation, and coefficient of

variation. It is seen that when there is a uniform distribution of reinforcement fraction from 0.16 to 0.56, the effective Young's modulus varies from 3.85 GPa to 9.26 GPa, with an average of 6.24 GPa and a coefficient of variation of 19.32%. On the other hand, the effective Poisson's ratio ranges from 0.31 to 0.39, with an average of 0.35 and a coefficient of variation of only 4.6%.
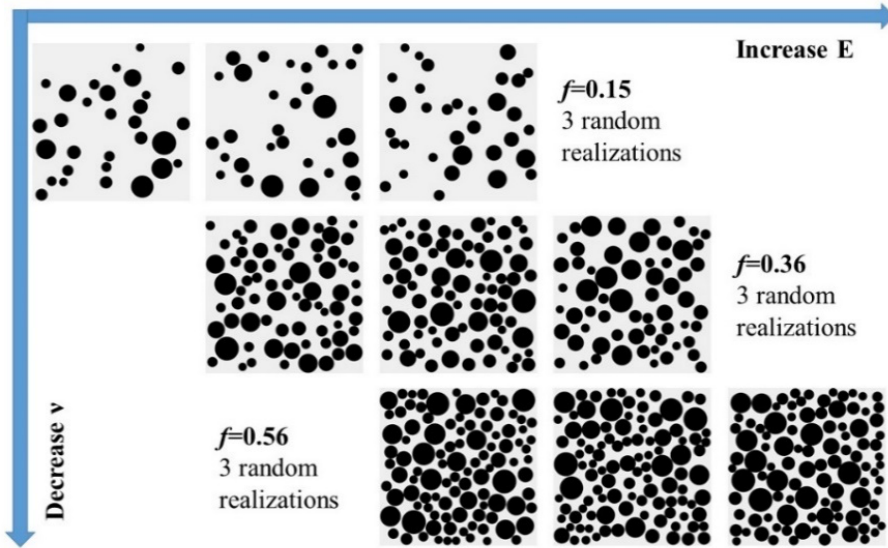
Fig. 5. Illustration of different random microstructures, in increasing the reinforcement fraction *f*
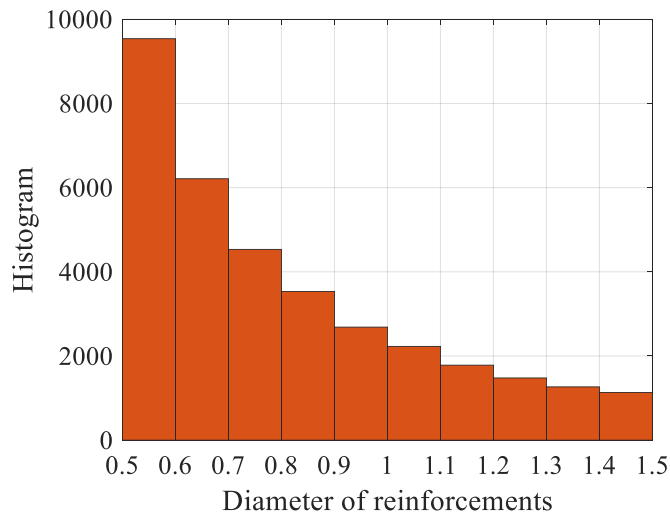
Fig. 6. Histogram of the diameter of reinforcements
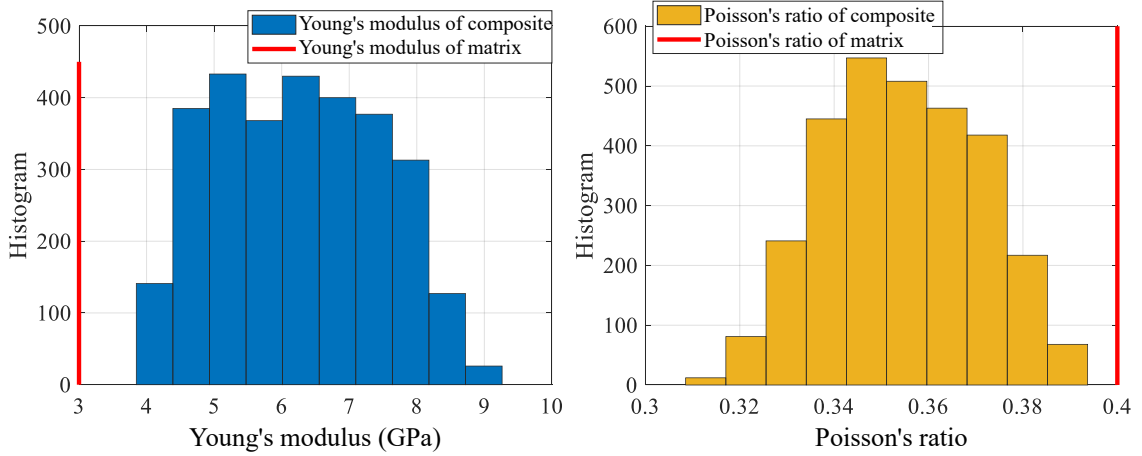
Fig. 7. Histogram of Young's modulus and Poisson's ratio of composite obtained from the finite element model (the figures also indicate the modulus of pure matrix)

Table 3. Statistical analysis of 3000 random microstructures

Parameter	Reinforcement fraction	Young's modulus of composite (GPa)	Poisson's ratio of composite	Number of inclusions in microstructure
Number of data points	3000	3000	3000	3000
Minimum	0.16	3.85	0.31	30
Q25	0.32	5.21	0.34	49
Median	0.41	6.24	0.35	71
Average	0.40	6.24	0.35	70
Q75	0.47	7.22	0.37	90
Maximum	0.56	9.26	0.39	110
Standard deviation	0.09	1.21	0.02	23
Coefficient of variation (%)	22.7	19.32	4.6	33

3.3. Training of CNN model for regression task

Using the microstructure images datastore previously introduced, a CNN model with 16 layers was trained using Matlab on a CPU AMD Ryzen Threadripper 3970X (3.7 GHz turbo up to 4.5 GHz), 96 GB RAM. The model was evaluated every iteration using the validation data points. Fig. 8 details the proposed CNN's architecture. Type, size of activations, weights, and bias parameters are also indicated in Fig. 8 for each layer. It should be noted that such an architecture was set based on Deep Network Designer application of Matlab.

LAYER INFORMATION

		Name	Type	Activations
	1	imageinput 510×510×1 images with 'zerocenter' nor...	Image Input	510(S) × 510(S) × 1(C) × 1(B)
	2	conv_1 8 3×3×1 convolutions with stride [1 1] an...	2-D Convolution	510(S) × 510(S) × 8(C) × 1(B)
	3	batchnorm_1 Batch normalization with 8 channels	Batch Normalization	510(S) × 510(S) × 8(C) × 1(B)
	4	relu_1 ReLU	ReLU	510(S) × 510(S) × 8(C) × 1(B)
	5	avgpool2d_1 2×2 average pooling with stride [2 2] an...	2-D Average Pooling	255(S) × 255(S) × 8(C) × 1(B)
	6	conv_2 16 3×3×8 convolutions with stride [1 1] a...	2-D Convolution	255(S) × 255(S) × 16(C) × 1(B)
	7	batchnorm_2 Batch normalization with 16 channels	Batch Normalization	255(S) × 255(S) × 16(C) × 1(B)
	8	relu_2 ReLU	ReLU	255(S) × 255(S) × 16(C) × 1(B)
	9	avgpool2d_2 2×2 average pooling with stride [2 2] an...	2-D Average Pooling	127(S) × 127(S) × 16(C) × 1(B)
	10	conv_3 32 3×3×16 convolutions with stride [1 1] ...	2-D Convolution	127(S) × 127(S) × 32(C) × 1(B)
	11	batchnorm_3 Batch normalization with 32 channels	Batch Normalization	127(S) × 127(S) × 32(C) × 1(B)
	12	relu_3 ReLU	ReLU	127(S) × 127(S) × 32(C) × 1(B)
	13	conv_4 32 3×3×32 convolutions with stride [1 1] ...	2-D Convolution	127(S) × 127(S) × 32(C) × 1(B)
	14	batchnorm_4 Batch normalization with 32 channels	Batch Normalization	127(S) × 127(S) × 32(C) × 1(B)
	15	relu_4 ReLU	ReLU	127(S) × 127(S) × 32(C) × 1(B)
	16	fc 2 fully connected layer	Fully Connected	2(C) × 1(B)

Fig. 8. Details of the architecture of the convolutional neural network model

Fig. 9 shows the training progress in terms of training loss and testing loss, respectively. It is seen in Fig. 9 that the training phase reaches convergence after about 80 iterations. Besides, good results of training loss and testing loss were also obtained, avoiding overfitting.

3.4. Prediction performance

Fig. 10 introduces regression graphs between actual and predicted moduli using the convolutional neural network model. It is indicated that for the prediction of Young's modulus, a correlation coefficient of 0.9643 and a linear fit of $y = x + 0.045$ were obtained. On the other hand, for the prediction of Poisson's ratio, a correlation coefficient of 0.9467 and a linear fit of $y = 0.99x - 0.028$ were obtained.
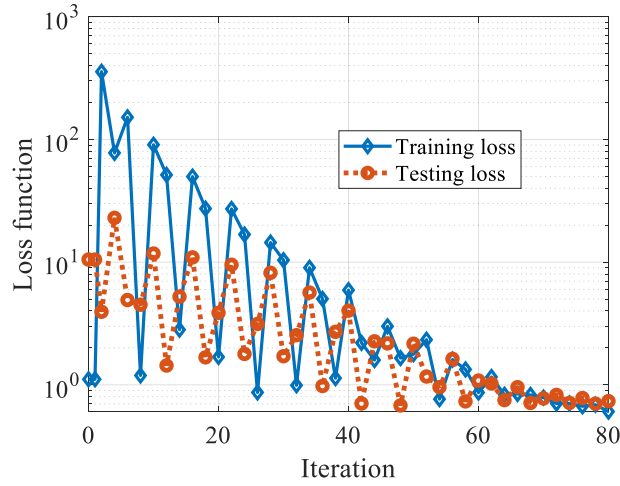
Fig. 9. Training and testing loss functions during the training of
the convolutional neural network model
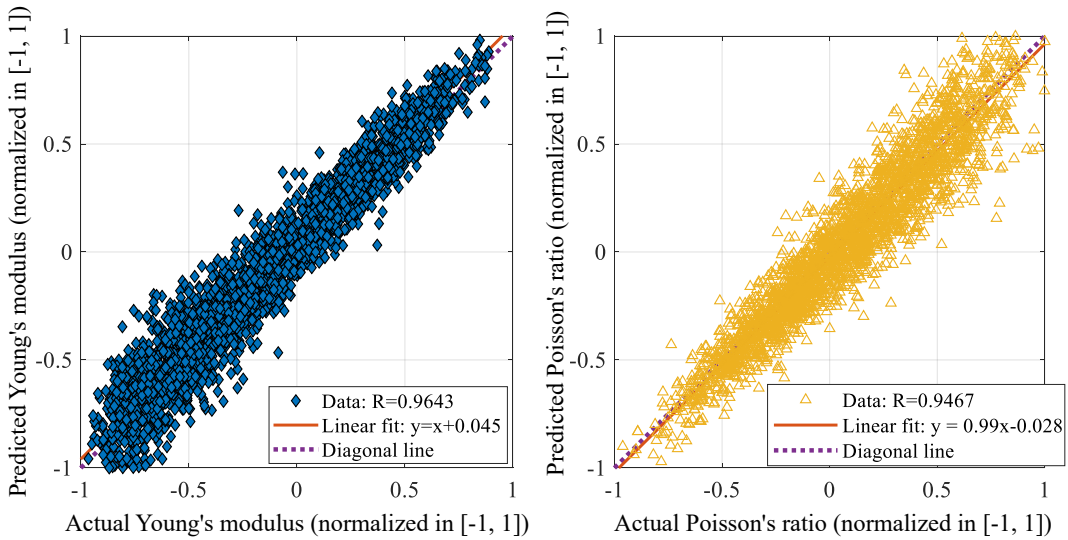
Fig. 10. Regression graphs between actual and predicted moduli using
the convolutional neural network model

Next, Fig. 11 provides a sensitivity analysis for different ranges of Young's modulus
of the composite, between the CNN and finite element model. The top plot of Fig. 11
illustrates the relationship between the reinforcement fraction f and the corresponding
Young's modulus of the composite material. The predicted values align closely with the

actual data, indicating that the CNN model effectively captures the nonlinear dependence of the composite's Young's modulus on the reinforcement fraction. The scatter of the data shows variability due to the random distribution of inclusions, but the trend remains consistent, suggesting reliable model performance.

The bottom plot of Fig. 11 presents the probability distributions of the composite's Young's modulus for various reinforcement fraction ranges. Both actual data (solid lines) and predicted data (dotted lines) are shown for comparison. For each range of f, the distributions of the predicted data closely match those of the actual data, further validating the accuracy of the CNN model. As the reinforcement fraction increases, the distributions shift toward higher Young's modulus values.
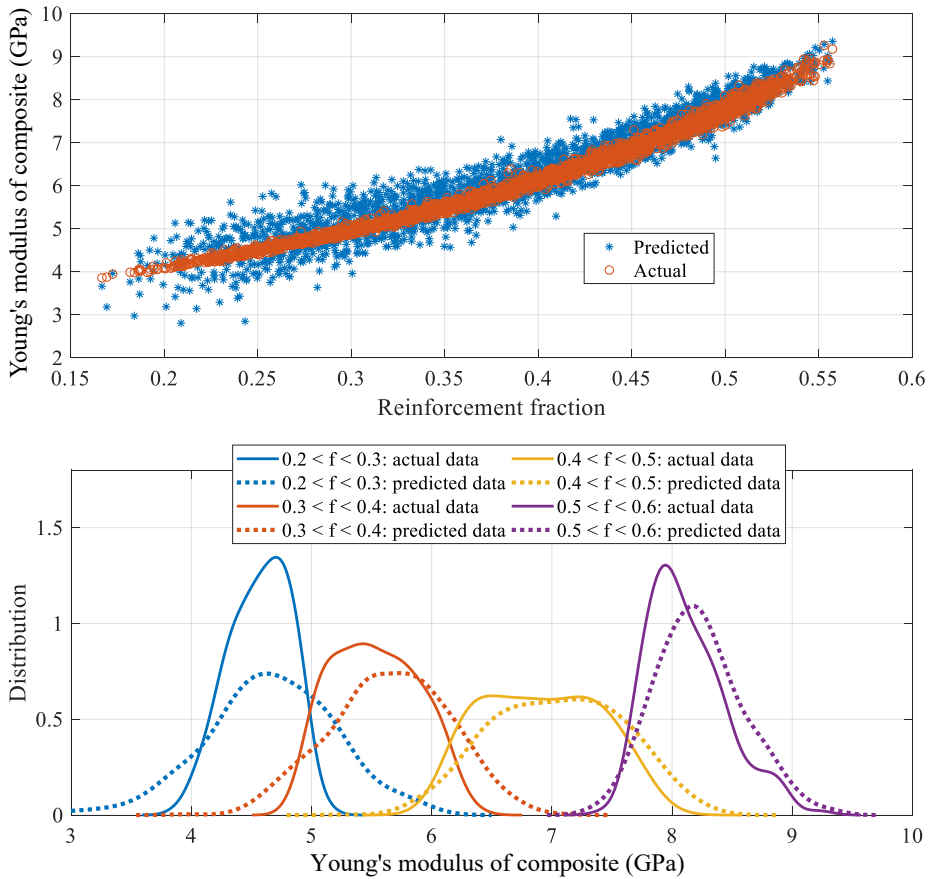
Fig. 11. Sensitivity analysis for different ranges of Young's modulus of the composite

4. CONCLUSION AND PERSPECTIVES

The main conclusions are summarized as below:

- This study developed a convolutional neural network (CNN) framework to predict the effective mechanical properties of particulate composite materials using finite element (FE) simulation data;

- The CNN model demonstrated high accuracy in predicting Young's modulus and Poisson's ratio while accounting for the random distribution of inclusions;

- The methodology effectively addressed challenges related to microstructural randomness in conventional homogenization techniques.

From a future perspective, this study opens several research directions. First, the incorporation of additional microstructural complexities, such as anisotropic inclusions, graded reinforcement, and interfacial effects, could enhance the model's applicability to a wider range of composite materials. Second, extending the framework to 3D microstructures would enable the homogenization of real-world composites with intricate geometries.

DECLARATION OF COMPETING INTEREST

The authors declare that they have no known competing financial interests or personal relationships that could have appeared to influence the work reported in this paper.

ACKNOWLEDGMENT

REFERENCES

[1] J. W. Ju and K. Yanase. Micromechanics and effective elastic moduli of particle-reinforced composites with near-field particle interactions. *Acta Mechanica*, **215**, (2010), pp. 135–153. https://doi.org/10.1007/s00707-010-0337-2.

[2] J. C. Smith. Experimental values for the elastic constants of a particulate-filled glassy polymer. *Journal of Research of the National Bureau of Standards Section A: Physics and Chemistry*, **80A**, (1976). https://doi.org/10.6028/jres.080a.008.

[3] B. Raju, S. R. Hiremath, and D. Roy Mahapatra. A review of micromechanics based models for effective elastic properties of reinforced polymer matrix composites. *Composite Structures*, **204**, (2018), pp. 607–619. https://doi.org/10.1016/j.compstruct.2018.07.125.

[4] M. Barral, G. Chatzigeorgiou, F. Meraghni, and R. Léon. Homogenization using modified Mori-Tanaka and TFA framework for elastoplastic-viscoelastic-viscoplastic composites: Theory and numerical validation. *International Journal of Plasticity*, **127**, (2020). https://doi.org/10.1016/j.ijplas.2019.11.011.

[5] S. Kanaun. An efficient homogenization method for composite materials with elastoplastic components. *International Journal of Engineering Science*, **57**, (2012), pp. 36–49. https://doi.org/10.1016/j.ijengsci.2012.04.005.

[6] X. Peng and J. Cao. A dual homogenization and finite element approach for material characterization of textile composites. *Composites Part B: Engineering*, **33**, (2002), pp. 45–56. https://doi.org/10.1016/s1359-8368(01)00052-x.

[7] L. Taut and V. Monchiet. Numerical homogenization with FFT method for elastic composites with spring-type interfaces. *Composite Structures*, **305**, (2023). https://doi.org/10.1016/j.compstruct.2022.116426.

[8] J. Jiang, J. Wu, Q. Chen, G. Chatzigeorgiou, and F. Meraghni. Physically informed deep homogenization neural network for unidirectional multiphase/multi-inclusion thermoconductive composites. *Computer Methods in Applied Mechanics and Engineering*, **409**, (2023). https://doi.org/10.1016/j.cma.2023.115972.

[9] F. Kibrete, T. Trzepieciński, H. S. Gebremedhen, and D. E. Woldemichael. Artificial intelligence in predicting mechanical properties of composite materials. *Journal of Composites Science*, **7**, (2023). https://doi.org/10.3390/jcs7090364.

[10] H. R. Bayat, B. Mustaq, and A. Vötterl. Predictive residual stress analysis in gear units: an artificial intelligence approach based on finite element data. *Advances in Mechanical Engineering*, **16**, (2024). https://doi.org/10.1177/16878132241290948.

[11] N. Altinkok and R. Koker. Neural network approach to prediction of bending strength and hardening behaviour of particulate reinforced (Al–Si–Mg)-aluminium matrix composites. *Materials & Design*, **25**, (2004), pp. 595–602. https://doi.org/10.1016/j.matdes.2004.02.014.

[12] R. Koker, N. Altinkok, and A. Demir. Neural network based prediction of mechanical properties of particulate reinforced metal matrix composites using various training algorithms. *Materials & Design*, **28**, (2007), pp. 616–627. https://doi.org/10.1016/j.matdes.2005.07.021.

[13] X. Li, Y. Zhang, H. Zhao, C. Burkhart, L. C. Brinson, and W. Chen. A transfer learning approach for microstructure reconstruction and structure-property predictions. *Scientific Reports*, **8**, (2018). https://doi.org/10.1038/s41598-018-31571-7.

[14] A. Henkes, I. Caylak, and R. Mahnken. A deep learning driven uncertain full-field homogenization method. *PAMM*, **20**, (2021). https://doi.org/10.1002/pamm.202000180.

[15] W. Wang, Y. Zhao, and Y. Li. Ensemble machine learning for predicting the homogenized elastic properties of unidirectional composites: A SHAP-based interpretability analysis. *Acta Mechanica Sinica*, **40**, (2023). https://doi.org/10.1007/s10409-023-23301-x.

[16] Y. Wang, C. Soutis, D. Ando, Y. Sutou, and F. Narita. Application of deep neural network learning in composites design. *European Journal of Materials*, **2**, (2022), pp. 117–170. https://doi.org/10.1080/26889277.2022.2053302.

[17] H. Ahmadi Moghaddam and P. Mertiny. Stochastic finite element analysis framework for modelling mechanical properties of particulate modified polymer composites. *Materials*, **12**, (2019). https://doi.org/10.3390/ma12172777.

[18] C. Rao and Y. Liu. Three-dimensional convolutional neural network (3D-CNN) for heterogeneous material homogenization. *Computational Materials Science*, **184**, (2020). https://doi.org/10.1016/j.commatsci.2020.109850.

[19] A. Valishin and N. Beriachvili. Applying neural networks to analyse the properties and structure of composite materials. In S. Kovačević and K. Kamyshev, editors, *E3S Web of Conferences*, EDP Sciences, Vol. 376, (2023). https://doi.org/10.1051/e3sconf/202337601041.